

## Article

# Conversion of Sugarcane Trash to Nanocrystalline Cellulose and its Life Cycle Assessment

Agung Wibowo<sup>1</sup>, Nutchapon Chiarasumran<sup>1</sup>, Anusith Thanapimmetha<sup>1,\*</sup>, Maythee Saisriyoot<sup>1</sup>, Penjit Srinophakun<sup>1,2,\*</sup>, Nopparat Suriyachai<sup>3</sup> and Verawat Champreda<sup>4</sup>

<sup>1</sup> Department of Engineering, Faculty of Engineering, Kasetsart University, Bangkok 10900, Thailand

<sup>2</sup> KU-Biodiesel Project, Chemical Engineering Department, Kasetsart University, Bangkok 10900, Thailand

<sup>3</sup> School of Energy and Environment, University of Phayao, Phayao 56000, Thailand

<sup>4</sup> Biorefinery Technology and Bioproducts Research Group, National Center for Genetic Engineering and Biotechnology, Pathumthani 12120, Thailand

\* Correspondence: fengjrc@ku.ac.th (A.T.); fengpjs@ku.ac.th (P.S.)

**Abstract:** Sugarcane trash (SCT) is a promising, underutilized raw material for producing value-added bio-based materials. Nanocrystalline cellulose (NCC) production conditions were obtained from the experiment. On the other hand, bioethanol production conditions were retrieved from the secondary data. This study compared the environmental impact of SCT in NCC production to that of bioethanol. For NCC production, SCT was subjected to organosolv pretreatment (140, 160, or 180 °C) in a mixed solvent system (methyl isobutyl ketone (MIBK), ethanol, and water), bleached, and then hydrolyzed with different concentrations of sulfuric acid (50 and 58%) for varying times. Organosolv pretreatment at 180 °C removed 98.24 and 81.15% of the hemicellulose and lignin, respectively, resulting in 73.51 and 79.72% cellulose purity and recovery. In addition, bleaching increased the cellulose purity to 95.42%. Field Emission Transmission Electron Microscopy (FE-TEM) analysis showed that NCC's small 2:1 elliptical particles were found at the hydrolysis of 50% H<sub>2</sub>SO<sub>4</sub> for 45 min. The X-ray diffraction (XRD) pattern revealed 70% crystalline index values for NCC obtained from 50% H<sub>2</sub>SO<sub>4</sub> with 45 min retention times. Then, the optimum conditions of NCC production were used for LCA analysis (Sigmapro software). The analysis included global warming, marine ecotoxicity, fresh water, and human carcinogenic toxicity. NCC production's electricity consumption (freeze-dried step) was the highest environmental impact on LCA analysis.

**Keywords:** sugarcane trash; organosolv pretreatment; nanocrystalline cellulose; life cycle assessment



**Citation:** Wibowo, A.; Chiarasumran, N.; Thanapimmetha, A.; Saisriyoot, M.; Srinophakun, P.; Suriyachai, N.; Champreda, V. Conversion of Sugarcane Trash to Nanocrystalline Cellulose and its Life Cycle Assessment. *Catalysts* **2022**, *12*, 1215. <https://doi.org/10.3390/catal12101215>

Academic Editors:  
Paripok Phitsuwan and  
Ken-Lin Chang

Received: 22 August 2022  
Accepted: 5 October 2022  
Published: 12 October 2022

**Publisher's Note:** MDPI stays neutral with regard to jurisdictional claims in published maps and institutional affiliations.



**Copyright:** © 2022 by the authors. Licensee MDPI, Basel, Switzerland. This article is an open access article distributed under the terms and conditions of the Creative Commons Attribution (CC BY) license (<https://creativecommons.org/licenses/by/4.0/>).

## 1. Introduction

Lignocellulosic biomass appears to be the most promising option as a renewable feedstock, generating energy and platform chemicals [1]. This kind of material consists of carbohydrate polymers (cellulose and hemicellulose, etc.) and non-carbohydrate phenolic polymers (lignin) [2]. The feedstock is abundant and non-edible [3,4]. Lignocellulose can come from many sources, such as agricultural wastes or crop residues, agro-industrial by-products, and municipal solid waste [5,6]. Notably, agricultural waste lignocellulosic materials are abundant in Thailand and Southeast Asian countries [7]. In Thailand, more than 100 million t of agricultural waste (mainly sugarcane and rice) is generated annually [8,9]. Cane waste has great potential to be developed continuously since this waste contains a large proportion of cellulose (32–44.55%), hemicelluloses (14–27.44%), and lignin (23–20.18%) [10,11]. Hence, this high fraction of cellulose makes cane waste an excellent raw material to be developed as NCC (nanocrystal cellulose) [12].

NCC materials have recently attracted much attention because they are abundant, renewable, non-toxic, and biodegradable [13]. Moreover, such material can be applied in water and wastewater treatment [14], tissue engineering [15], and packaging [16]. As a result, the global demand for the nano-cellulose market size is foreseen to achieve USD

783 million by 2025 [17]. In addition, cane waste can be converted into bioethanol as a necessary renewable fuel to reduce carbon dioxide emissions [18–21]. In contrast, this work investigated the production of NCC, which began with biomass pretreatment using the acid catalyst and decomposed into cellulose, lignin, and hemicellulose [12]. Then, a life cycle assessment (LCA) is performed to determine NCC production using energy consumption and total products.

## 2. Results and Discussion

### 2.1. Effects of Reaction Temperature and Catalyst for Organosolv Pretreatment

The untreated sugarcane trash (SCT) was initially characterized to assess material conditions before undergoing the organosolv pretreatment [22]. The results of the characterization and organosolv pretreatment are shown in Table 1. It was found that the mean ( $\pm$ standard deviation) percentages of cellulose, hemicellulose, lignin, and ash were  $33.35 \pm 0.2$ ,  $20.26 \pm 0.4$ ,  $22.70 \pm 0.8$ , and  $7.13 \pm 0.1\%$ , respectively, which were similar to those reported by Powar et al. [10] and Cardoen et al. [11]. After pretreatment and bleaching (Table 1), 76.22% cellulose in the pretreated, bleached SCT made it a potential NCC production source. The organosolv pretreatment of SCT was conducted using 25, 42, and 33 v/v% of methyl isobutyl ketone (MIBK), ethanol, and water, respectively, with 0.05 M sulfuric acid as the catalyst. The reaction contained 100 mL of working volume, with the pretreatment temperature varying from 140 to 180 °C for 40 min. H<sub>2</sub>SO<sub>4</sub> was chosen as the catalyst in most clean fractionation processes reported due to its cost-effectiveness. In addition, this acid catalyst could increase the solubilization of hemicellulose and lignin [23]. Therefore, MIBK was selected as the solvent and washing agent since this reagent has high lignin solubility (more than 90%) and results in the enrichment of cellulose in the solid fraction [23].

The pretreatment temperature significantly influenced the delignification. When the pretreatment temperature increased from 140 to 180 °C, the lignin removal improved from 66.99 to 81.15%. A higher pretreatment temperature could provide more energy to facilitate the cleavage of lignin bonds, resulting in higher lignin removal [24]. Similarly, these trends occurred for the hemicellulose composition. As the temperature rose from 160 to 180 °C, the hemicellulose removal efficiency increased from 83.83% to 98.24%. Removing hemicelluloses involves the cleavage of covalent bonds that link hemicelluloses to lignin [25].

On the other hand, the cellulose recovery declined gradually to 79.72%, from 97.56% when the temperature rose from 140 to 180 °C. The reduction of cellulose recovery because the cleavage of the glycosidic bonds influences the declining cellulose recovery and the hydrolysis of cellulose to glucose and cello-oligosaccharides [26]. Conversely, the percentage of cellulose purity increased gradually from 66.60 to 73.51% when the temperature was enhanced from 140 to 180 °C.

Out of these results, the optimum pretreatment temperature at 180 °C was fixed for a further experiment, which recorded the lignin composition at 11.01%, with 79.92% cellulose recovery and 98.24% hemicellulose removal efficiency. The temperature of 180 °C was selected because it produced the highest cellulose purity (73.51%). Figure 1 shows the appearance of the SCT samples, which became darker compared to untreated SCT as the temperature increased (Figure 1a,d).



**Figure 1.** Appearance comparison of (a) untreated SCT, (b) pretreated SCT at 140 °C, (c) pretreated SCT at 160 °C, (d) pretreated SCT at 180 °C and (e) pretreated and bleached SCT (PB-SCT).

**Table 1.** Compositions of untreated SCT, treated SCT at different temperatures and treated and bleached SCT (PB-SCT).

Temperature (°C)	Solid Yield (%)	Pulp Composition (%)				Cellulose Recovery (%)	Removal Efficiency (%)		Cellulose Purity (%)
		Cellulose	Lignin	Hemicellulose	Ash		Hemicellulose	Lignin	
Untreated SCT	-	33.35 ± 0.2	22.70 ± 0.8	20.26 ± 0.4	7.13 ± 0.1	-	-	-	-
140	46.4 ± 0.26	63.20 ± 2.6	14.47 ± 1.3	7.90 ± 0.5	9.33 ± 0.4	97.56 ± 4.0	83.83 ± 1.8	66.99 ± 1.5	66.60 ± 0.5
160	41.6 ± 0.18	64.45 ± 2.8	11.66 ± 0.6	4.63 ± 0.3	11.54 ± 0.8	89.09 ± 1.2	91.54 ± 0.5	76.08 ± 2.1	69.82 ± 1.7
180	34.7 ± 0.08	69.04 ± 0.1	11.01 ± 0.6	1.14 ± 0.4	12.73 ± 0.2	79.92 ± 1.3	98.24 ± 1.0	81.15 ± 1.3	73.51 ± 1.1
Pretreated and Bleached SCT (PB-SCT)	18.2 ± 0.05	76.22 ± 1.5	3.05 ± 0.9	0.15 ± 0.02	0.47 ± 0.1	27.94 ± 0.7	99.92 ± 0.01	98.48 ± 0.4	95.42 ± 1.1

## 2.2. Bleaching

The bleaching step aims to raise cellulose purity after the cane trash undergoes organo-solv pretreatment [27]. The  $H_2O_2$  in the base conditions was used for this experiment. The lignin removal increased from 81.15 to 98.48% (Table 1), and cellulose purity rose sharply from 73.51 to 95.42%. Conversely, the amount of cellulose recovery was substantially reduced to 27.94%. The increased lignin removal shows the effectiveness of the bleaching reaction. However, the radicals generated may randomly cause alkaline-catalyzed cleavages of polysaccharide chains [28], leading to cellulose degradation [29]. The appearance of pretreated and bleached SCT (PB-SCT) seems to be whiter than the pretreated SCT (Figure 1). The color change might imply increased and decreased cellulose and lignin content [30].

## 2.3. Morphological Analysis

Hydrolysis of the PB-SCT was studied using 50% and 58% sulfuric acid at 45 °C for 30 min, 45 min, and 60 min. The hydrolysate became a darker brown after 30 min of hydrolysis using 58% sulfuric. This dark color may have resulted from side reactions, such as dehydration [31,32]. Figure 2 shows the particle size of the hydrolysis product. The average particle size was estimated to visualize the trend of the changes in particle sizes. The obtained NCC seemed to have a 2:1 elliptical shape, with an average of 96 nm length and an average of 45 nm diameter for the NCC from hydrolysis reactions with 50% sulfuric acid for 45 min. The size of NCC was smaller at a longer hydrolysis time of 60 min, and NCC became spherical with an average diameter of 38 nm. Acid hydrolysis during the longer reaction time eliminates the amorphous regions and portions of the crystalline component and reduces the crystallite sizes [33,34]. Various diameters of spherical NCC from agricultural waste were produced, including 95.9 nm [35], 30–40 nm [36], 42–82 nm [37], and 33–67 nm [38].

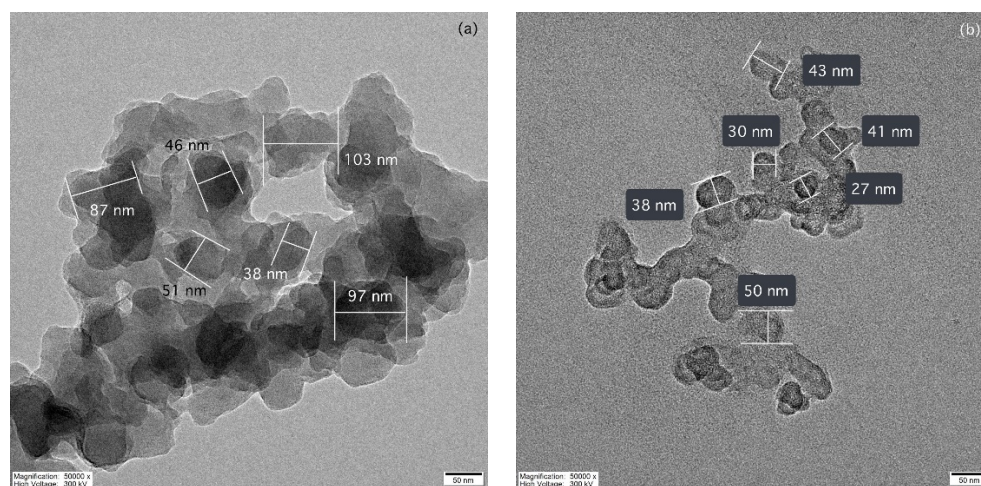


**Figure 2.** FE-TEM images of (a) 50%  $H_2SO_4$  for 45 min, (b) 50%  $H_2SO_4$  for 60 min.

Interestingly, the coagulation between particles was found even though samples were split by suspending them in water before being pipetted onto the FE-TEM grid [37]. Expectedly, the impurity of a sulfated group ( $S-O_2$ ) from acid hydrolysis might cause this coagulation. However, sulfuric acid was chosen for hydrolysis since it can produce smaller NCC [38] and also can effectively hydrolyze amorphous regions completely [39] with a higher crystallinity index [33]. In addition, sonication was carried out for 10 min at the end of hydrolysis in ice to decrease the nanocellulose particle size and avoid overheating. On the other hand, sonication longer than 10 min can cause some degradation of the NCC [40].

#### 2.4. X-ray Diffraction Analysis (XRD)

The XRD patterns of samples subjected to 50% H<sub>2</sub>SO<sub>4</sub> for 45 min and 60 min hydrolysis are presented in Figure 3. The diffractograms showed two diffraction angles at 2 $\theta$  of about 15° and 22°, indicating the typical native cellulose structure (cellulose I) [41,42]. In addition, diffraction angles at around 18° and 22° were noted as the NCC's amorphous and crystal regions [42]. The peak at approximately 2 $\theta$  = 22° appeared sharper and more substantial and indicated the crystalline domain [43]. However, the border crystal peak was also found [44]. The XRD pattern showed that at 2 $\theta$  = 22°, there were intensities of 15,134 and 9420. At the same time, the levels were 4533 and 3455 for 2 $\theta$  = 18° for 50% H<sub>2</sub>SO<sub>4</sub> at 45 and 60 min, respectively. Of these 2 $\theta$  intensities, the crystallinity indexes of NCC with 50% H<sub>2</sub>SO<sub>4</sub> for 45 and 60 min were 70% and 63%, respectively. However, the changing percentage of the crystallinity index was associated with the hydrolysis condition. Kargarzadeh et al. [43] reported that a further increase in the hydrolysis time could lead to a decrease in the NCC shape and a decline in the NCC crystallinity.

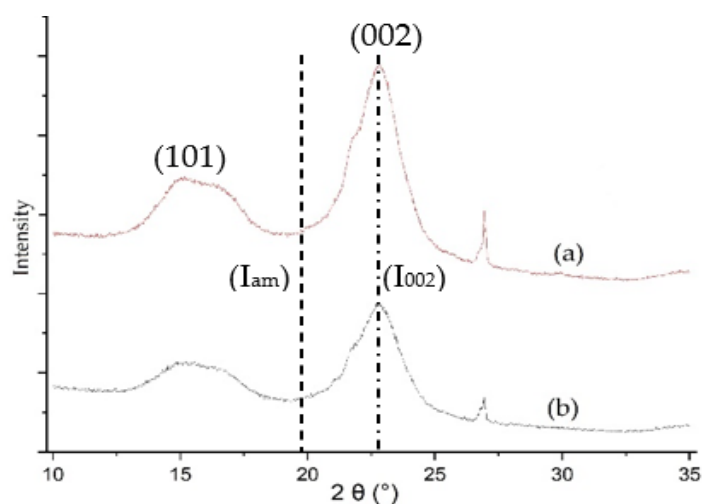


**Figure 3.** NCC XRD diffractograms of (a) 50% H<sub>2</sub>SO<sub>4</sub> for 45 min NCC and (b) 50% H<sub>2</sub>SO<sub>4</sub> for 60 min.

#### 2.5. Fourier-Transform Infrared Spectroscopy (FTIR) Characterization

Figure 4 shows the FTIR spectra of NCC after undergoing hydrolysis with 50% H<sub>2</sub>SO<sub>4</sub> for 45 mins and 60 mins, respectively. Overall, both samples exhibit almost identical spectra, indicating no changes in their chemical composition during sulfuric acid hydrolysis [45]. The absorbance peaks in the 3500–3200 cm<sup>-1</sup> are associated with the vibration of a hydroxyl group (–OH) stretching of cellulose due to intra- and intermolecular hydrogen bonds. In addition, the peaks around 2900–2800 cm<sup>-1</sup> can correspond with C–H stretching vibration in cellulose and hemicellulose. The attribution to the C=O stretching of uranic esters and acetyl groups of the hemicellulose occurred at 1733 cm<sup>-1</sup>. The exact peak also represented ester linkages of the carboxylic group in hemicellulose and lignin [45]. The prominent band at 1640 cm<sup>-1</sup> was attributed to the O–H of the absorbed water [42,46]. The peaks at 1428 and 1370 cm<sup>-1</sup> correlated with the –CH<sub>2</sub> scissoring motion of cellulose and C–H bending, respectively [47]. The carbonyl group's vibration peaked at 1322 cm<sup>-1</sup> [45]. The existence of a sulfated group (S–O<sub>2</sub>) at 1160 cm<sup>-1</sup> was referred to as sulfuric acid from cellulose hydrolysis [48]. A peak at 1111 cm<sup>-1</sup> reflected glucose ring stretching [49,50], 1060 cm<sup>-1</sup> with the vibration of C–O–C in the pyranose ring [35], and 897 cm<sup>-1</sup> with C–O–C extension at  $\beta$ -glycosidic linkages between glucose [51].

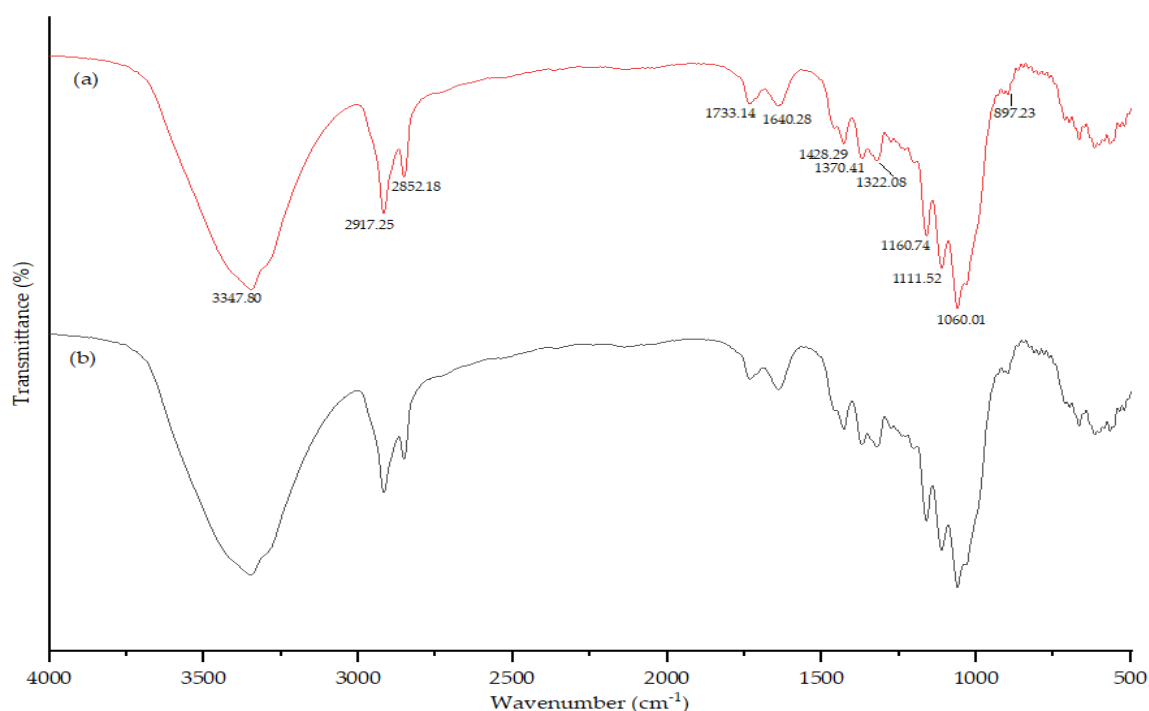


**Figure 4.** FTIR spectra of (a) 50% H<sub>2</sub>SO<sub>4</sub> for 45 min NCC and (b) 50% H<sub>2</sub>SO<sub>4</sub> for 60 min.

## 2.6. Life Cycle Impact Assessment

### 2.6.1. Global Warming Impact on NCC Production

Figure 5 shows that 174.6 kg of CO<sub>2</sub> eq was produced from 1 kg of SCT or for the production of 0.011 kg of NCC, most of which was contributed by power and MIBK with 136.6 and 31.4 kg CO<sub>2</sub> eq, respectively. The high impact of electricity contribution to global warming was related to the high electricity usage (667.6 MJ) and electricity generation, in which 90% of electricity generation is produced from fossil fuel [52]. In addition, fossil fuel contributes to global warming due to the carbon dioxide (CO<sub>2</sub>) released during fossil-fuel combustion [53]. The enormous MIBK contribution relates to the high chemical quantity. On the other hand, MIBK is a volatile organic compound that is well known as one of the significant contributors to air pollution [54] and global warming impact [55]. The other remaining consequences, which need more attention, are freshwater and marine ecotoxicity because of the high amount of wastewater (Table 2) during NCC production.

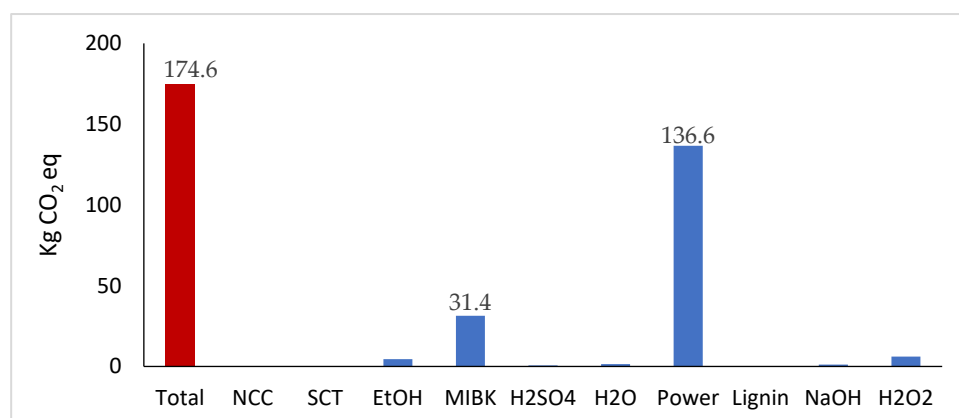


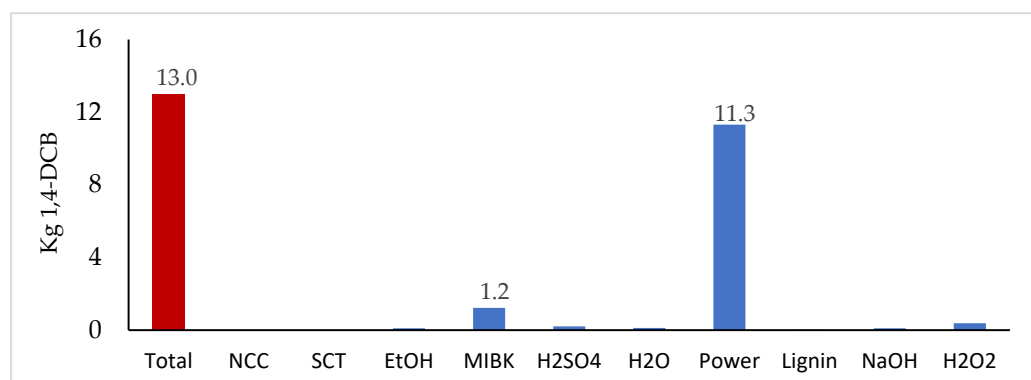
**Figure 5.** The global warming impact of NCC production using ReCipe Midpoint (H).

**Table 2.** Life cycle inventory of NCC production.

No	Process	Input		Output	
		Feeding	Amount	Product	Amount (Kg)
1	Pretreatment	MIBK (Kg)	6.82	Pulp	0.35
		Ethanol (Kg)	3.31	Lignin	0.16
		H <sub>2</sub> SO <sub>4</sub> (Kg)	0.04	Water	1.1
		SCT (Kg)	1	Waste vapor	6.74
		Water (Kg)	49.89	Wastewater	52.69
		Energy (J)	$1.0 \times 10^7$		
2	Bleaching	Pretreated SCT (Kg)	0.35	Pulp bleached	0.1818
		NaOH (Kg)	0.844	H <sub>2</sub> O	0.517
		H <sub>2</sub> O <sub>2</sub> (Kg)	3.997	Wastewater	66.292
		H <sub>2</sub> O (Kg)	61.79		
		Energy (J)	$3.6 \times 10^6$		
3	Extraction and Sonication	PB-SCT (Kg)	0.1818	NCC suspension	1.14
		H <sub>2</sub> SO <sub>4</sub> (Kg)	4.158675	Wastewater	825.833
		H <sub>2</sub> O (Kg)	822.632		
		Energy (J)	$6.1 \times 10^5$		
4	Freeze-drying	NCC suspension (Kg)	1.14	NCC	0.011
		Energy (j)	$6.5 \times 10^8$		1.13

### 2.6.2. Marine Ecotoxicity Impact of NCC Production

Generally, Figure 6 depicts that 13.0 kg of 1,4-DCB contributed to the marine ecotoxicity impact by NCC production, most of which was due to power (11.3 kg 1,4-DCB) and MIBK (1.2 kg 1,4 DCB). The high contribution of electricity toward marine ecotoxicity was related to the metals generated (such as Se, Ni, and Cu) during fossil fuel burning, in which most of these metals will end up in the water and poison the marine ecosystem [56]. The high impact of MIBK on marine ecotoxicity causes massive usage. Although MIBK has low toxicity toward microorganisms and aquatic organisms [57], Chipman [58] reported that inappropriate disposal in large quantities could cause toxicity to organisms in the environment.

**Figure 6.** Marine ecotoxicity of NCC production using ReCipe Midpoint (H).

### 2.6.3. Freshwater Ecotoxicity Impact of NCC Production

Broadly, Figure 7 explains that in producing 0.011 kg of NCC, 10.4 kg of 1,4-DCB was exposed to freshwater damage. MIBK and power made more substantial contributions of 1.0 and 8.9 kg 1,4-DCB, respectively. The considerable freshwater impact from electricity was caused by the high number of metals (such as Cu, Se, and Ba) generated during fossil fuel combustion that is consequently in water [56] as pollutants. Coal constitutes the second-largest share of the electricity output (22%) in Thailand, and according to Atilgan and Azapagic [59], coal power is associated with ecotoxicities (marine and freshwater).

MIBK is considered a volatile organic compound [54] that can interact with the other pollutants (NO<sub>x</sub> and SO<sub>x</sub>) in the atmosphere and atmospheric water, resulting in dry deposition and wet deposition [60]. These depositions then flow and end up in the water catchment, polluting the freshwater ecosystem. The last impact that needs to be assessed is human carcinogenic toxicity.

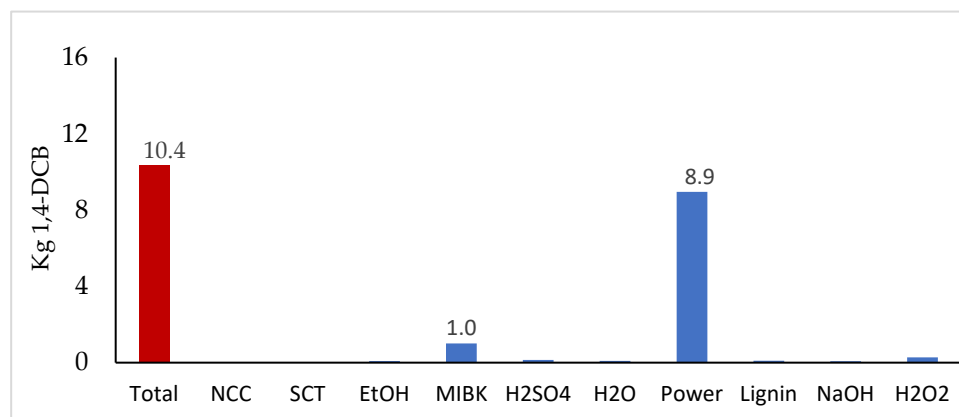


**Figure 7.** Freshwater ecotoxicity impact of NCC production using ReCipe Midpoint (H).

#### 2.6.4. Human Carcinogenic Toxicity Impact of NCC Production

Figure 8 shows that 7.4 kg of 1,4-DCB was produced during the production of 0.011 kg of NCC, with power making the most significant contribution, followed by MIBK of 5.5 and 0.8 kg of 1,4-DCB, respectively. The considerable electricity impact is rendered by pollutants emitted (SO<sub>x</sub> and NO<sub>x</sub>) from fossil fuel combustion [61]. As a result, the population can be exposed to these contaminants that are potentially carcinogenic for humans through ingestion, inhalation, and dermal contact [62]. MIBK's more considerable contribution is that this chemical evaporates quickly at room temperature. Consequently, inhalation exposes people to this solvent, causing nose and lung irritation [63].

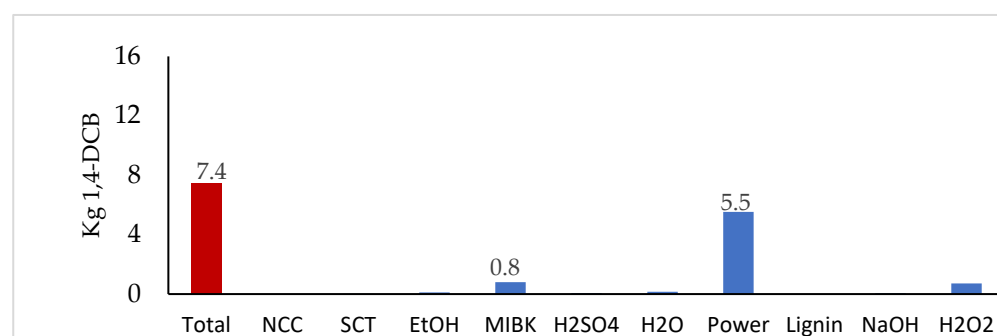


**Figure 8.** Human carcinogenic toxicity of NCC production using ReCipe Midpoint (H).

Power invariably causes the most significant environmental impact of these four categories (global warming, marine ecotoxicity, freshwater ecotoxicity, and human carcinogenic toxicity). All the production steps for NCC (Table 2) require energy. However, the freeze-dried process consumes the highest power of 651.92 MJ among those steps. The four impact analyses show that NCC production produces high environmental impacts (174.6 kg CO<sub>2</sub> eq, 13.0 kg 1,4-DCB, 10.4 kg 1,4-DCB, and 7.4 kg 1,4-DCB for global warming, marine ecotoxicity, freshwater ecotoxicity, and human carcinogenic toxicity impact, respectively).

### 3. Materials and Methods

#### 3.1. Materials

The dried SCT, supplied by a sugar mill in Thailand, was milled and sieved to 0.5–1.0 mm. The chemical composition was analyzed using the NREL method [64], which is based on the acid hydrolysis principle in which 0.3 g of the sample was hydrolyzed using 3 mL of 72% sulfuric acid for 2 h with vortex mixing every 15 min. Then, 84 mL of deionized water was added to the solution immediately, followed by autoclaving at 121 °C for 1 h. Cellulose and hemicellulose were determined from the liquid fraction, which had been neutralized using CaCO<sub>3</sub> that was analyzed using HPLC (Shimadzu, Kyoto, Japan) equipped with an Aminex HPX-87H (Biorad, Hercules, CA, USA) column and a refractive index detector (RID). Lignin was determined from the solid heating fraction at 105 °C for 4 h, then burnt at 575 °C for 2 h [65].

#### 3.2. Pretreatment Using Acid Catalyst

The biomass (10% *w/v*) was pretreated in a ternary solvent comprising MIBK, ethanol, and water (25, 42, and 33% *v/v*, respectively) with 0.05 M H<sub>2</sub>SO<sub>4</sub> as a catalyst for 140, 160, and 180 °C for 40 min with an initial pressure of nitrogen at 20 bars and stirring at 100 rpm in a 1 L high-pressure batch reactor (Parr Instruments, Moline, IL, USA) [23]. First, the reaction was stopped by quenching in an ice bath. Then, the slurry was passed through 20–25 µm filter paper. Finally, the residue was immersed in 30 mL of MIBK, filtered, neutralized with DI water, and dried at 70 °C in a hot-air oven. The pretreated SCT pulp yield was calculated as follows:

$$\text{Pulp Yield (\%)} = (f \text{ (g)} \times 100) \div i \text{ (g)} \quad (1)$$

where the pulp yield is the percentage of the remaining sample compared to the initial weight (%), and *f* and *i* are the weights of the remaining solid samples after the organosolv treatment and the initial raw material, respectively. The biomass compositions were determined based on the remaining contents in solid residues compared with the respective contents in the native biomass. The liquid fraction of the aqueous–organic mixture was separated into two phases by adding water in a separator funnel. Afterwards, the mixture was left at room temperature for 20 min for complete phase separation. The organic phase, which contained lignin and MIBK (the major component), was evaporated at 70 °C to recover lignin.

#### 3.3. NCC Production

##### 3.3.1. Bleaching

The pretreated SCT was mixed with 4% NaOH (1:2 *w/v*) [27]. Afterwards, 24% of H<sub>2</sub>O<sub>2</sub> (1:2 *w/v*) was slowly added; then, the mixtures were heated at 70 °C for 40 min with stirring. The bleached pulp (PB-SCT) was washed with DI water until neutral.

##### 3.3.2. Extraction

The PB-SCT were extracted using 50% and 58% sulfuric acid (1:25 *w/v*) at 45 °C and 350 rpm for 30, 45, and 60 min [27]. A ten-fold amount of cold DI water was added to the suspension. The mixture was centrifuged at 8000 rpm for 20 min and dialyzed against DI water. The solid fraction was recovered using centrifugation at 8000 rpm for 60 min. Finally, the particles were treated using sonication at 20 kHz for 10 min with 40% amplitude. Some NCC suspension was separated for particle analysis, and another suspension sample was freeze-dried (FD) to remove the water content [66].

##### 3.3.3. Characterization Procedures

The total yield of the NCC synthesis was calculated as a percentage ratio of the freeze-dried NCC based on the initial weight of cellulose in the raw material. Several instruments

were used to analyze the physicochemical properties: an FE-TEM, a Fourier-transform infrared spectroscope (FTIR), and an X-ray diffractometer (XRD).

The FE-TEM preparation was conducted by diluting 0.1–0.3% *w/w* of NCC in water. Then, one drop of each sample was deposited on a formvar or carbon-coated grid. After 1 min, the water drop was removed by dabbing it with tissue paper [67]. The FE-SEM micrographs were recorded at 40,000× magnification. The ImageJ unit estimated the sample diameter [37]. X-ray diffraction patterns were obtained using a D/max-2500 X-ray diffractometer (RigakuDenki, Tokyo, Japan) using Cu-K radiation (0.154 nm) in  $2\theta = 5\text{--}40^\circ$  at a scan rate of  $2^\circ/\text{min}$ . The crystallinity indices ( $I_c$ ) were counted based on the Segal method [68]:

$$I_c = \frac{I_{002} - I_{am}}{I_{002}} \times 100\% \quad (2)$$

where  $I_{002}$  and  $I_{am}$  are the peak intensities of the crystalline and amorphous materials, respectively, FT-IR was used to study the presence of chemical groups. Each sample was mixed with KBr. Their spectra were recorded at a resolution of  $2\text{ cm}^{-1}$  with a spectral range of  $4000\text{--}450\text{ cm}^{-1}$  [36].

### 3.4. Life Cycle Assessment

The NCC production was assessed for its environmental impact based on the product life cycle. The evaluation commenced by determining the energy consumption, raw material input, and output per functional unit using the SimaPro Software. Afterwards, the life cycle impact assessment procedure, based on the Ecoinvent database, was applied to calculate the environmental impact according to ReCiPe 2016 Midpoint/Endpoint (H) V1.04/World (2010).

#### 3.4.1. Goal and Scope Definition

The LCA study evaluated the environmental impact assessment of NCC production from sugar cane trash (SCT). The functional unit of cellulose extraction was 1 kg of SCT for NCC production. A total of 1 kg of SCT was converted to 0.011 kg NCC. Gate-to-gate was selected for the system boundary of these experiments. The system began with SCT grinding and organosolv pretreatment (using an  $\text{H}_2\text{SO}_4$  catalyst) to obtain cellulose and lignin, followed by bleaching, extraction, sonication, and freeze-drying.

#### 3.4.2. Life Cycle Inventory

The life cycle inventory data, including each stage of the NCC production process, are exhibited in Table 2. In addition, data regarding water consumption, electricity, and reagents were measured in the laboratory.

## 4. Conclusions

In this study, we determined the environmental impact of two processes using SCT as a raw material. At first, SCT was pretreated by organosolv using an acid catalyst and then used in NCC production. Next, the optimum conditions of NCC production were obtained by an experiment consisting of three steps: bleaching, extraction and sonication, and freeze-drying. Finally, the LCA of the process was analyzed. It was found that NCC production had the most significant severe environmental damage from electricity used in freeze-drying. This finding is essential for the future development of NCC production.

**Author Contributions:** The specified contributions of the authors were: conceptualization, P.S., A.T. and V.C.; methodology, A.W., A.T., N.S., V.C. and P.S.; software, N.S. and M.S.; validation, A.W., N.S., M.S. and A.T.; formal analysis, A.W., P.S., A.T. and N.C.; investigation, A.W., A.T., V.C. and P.S.; resources, N.S., M.S. and A.T.; data curation, all authors; writing—original draft preparation, A.W. and P.S.; writing—review and editing, P.S.; visualization, all authors; supervision, V.C. and P.S.; project administration, P.S.; funding acquisition, P.S. and V.C. All authors have read and agreed to the published version of the manuscript.

**Funding:** This research was partially funded by the National Science and Technology Development Agency (NSTDA) (p18-51760).

**Data Availability Statement:** The data was in the project's report, not available to the public.

**Acknowledgments:** The authors sincerely thank the Thailand Advanced Institute of Science and Technology-Tokyo Institute of Technology (TAIST-Tokyo Tech) for providing a scholarship and the KU-biodiesel project, Department of Chemical Engineering, Kasetsart University, for the financial support for the chemical analysis.

**Conflicts of Interest:** The authors declare no conflict of interest.

## References

1. Walter, D.; Virender, K.S.; Mengshan, L.; Govind, N.; Rajender, S.V. Lignocellulosic Biomass Transformations via Greener Oxidative Pretreatment Processes: Access to Energy and Value-Added Chemicals. *Front. Chem.* **2018**, *6*, 141.
2. Abdel-Hamid, A.M.; Solbiati, J.O.; Cann, I.K.O. Chapter one: Insights into lignin degradation and its potential industrial applications. In *Advances in Applied Microbiology*; Sariaslani, S., Gadd, G.M., Eds.; Elsevier Press: Amsterdam, The Netherlands, 2013; pp. 1–28. [\[CrossRef\]](#)
3. Mishra, R.K.; Mohanty, K. Characterization of non-edible lignocellulosic biomass in terms of their candidacy towards alternative renewable fuels. *Biomass Convers. Biorefinery* **2018**, *8*, 799–812. [\[CrossRef\]](#)
4. Ravindran, R.; Jaiswal, A.K. A comprehensive review on pretreatment strategy for lignocellulosic food industry waste: Challenges and opportunities. *Bioresour. Technol.* **2016**, *199*, 92–102. [\[CrossRef\]](#)
5. Limayem, A.; Ricke, S.C. Lignocellulosic biomass for bioethanol production: Current perspectives, potential issues and future prospects. *Prog. Energy Combust. Sci.* **2012**, *38*, 449–467. [\[CrossRef\]](#)
6. Sánchez, Ó.J.; Cardona, C.A. Trends in biotechnological production of fuel ethanol from different feedstocks. *Bioresour. Technol.* **2008**, *99*, 5270–5295. [\[CrossRef\]](#) [\[PubMed\]](#)
7. Maw Maw, T.; Dagmar, J.; Myo Min, W.; Aung Myat, T.; Tomáš, P. Biomass Energy: An Overview of Biomass Sources, Energy Potential, and Management in Southeast Asian Countries. *Resources* **2019**, *8*, 81.
8. Jimén, D.J.; Dini-Andreote, F.; Van Elsas, J.D. Metataxonomic profiling and prediction of functional behaviour of wheat straw degrading microbial consortia. *Biotechnol. Biofuels* **2014**, *7*, 2–30.
9. Photphisutthiphong, Y.; Vatanyoopaissarn, S. Dyadobacter and Sphingobacterium isolated from herbivore manure in Thailand and their cellulolytic activity in various organic waste substrates. *Agric. Nat. Resour.* **2019**, *53*, 89–98.
10. Powar, R.V.; Mehetre, S.A.; Powar, T.R.; Patil, S.B. End-Use Applications of Sugarcane Trash: A Comprehensive Review. *Sugar. Tech.* **2022**, *24*, 699–714. [\[CrossRef\]](#)
11. Cardoen, D.; Joshi, P.; Diels, L.; Sarma, P.M.; Pant, D. Agriculture biomass in India: Part 1. Estimation and characterization. *Resour. Conserv. Recycl.* **2015**, *102*, 39–48. [\[CrossRef\]](#)
12. Salimi, S.; Sotudeh-Gharebagh, R.; Zarghami, R.; Chan, S.Y.; Yuen, K.H. Production of Nanocellulose and Its Applications in Drug Delivery: A Critical Review. *ACS Sustain. Chem. Eng.* **2019**, *7*, 15800–15827. [\[CrossRef\]](#)
13. Thomas, B.; Raj, M.C.; Athira, K.B.; Rubiah, M.H.; Joy, J.; Moores, A.; Drisko, G.L.; Sanchez, C. Nanocellulose, a Versatile Green Platform: From Biosources to Materials and Their Applications. *Chem. Rev.* **2018**, *118*, 11575–11625. [\[CrossRef\]](#) [\[PubMed\]](#)
14. Carpenter, A.W.; De Lannoy, C.F.; Wiesner, M.R. Cellulose Nanomaterials in Water Treatment Technologies. *Environ. Sci. Technol.* **2015**, *49*, 5277–5287. [\[CrossRef\]](#)
15. Manhas, N.; Balasubramanian, K.; Prajith, P.; Rule, P.; Nimje, S. PCL/PVA Nanoencapsulated Reinforcing Fillers of Steam Exploded/Autoclaved Cellulose Nanofibrils for Tissue Engineering Applications. *RSC Adv.* **2015**, *5*, 23999–24008. [\[CrossRef\]](#)
16. Vilarinho, F.; Sanches Silva, A.; Vaz, M.F.; Farinha, J.P. Nanocellulose in green food packaging. *Crit. Rev. Food Sci. Nutr.* **2018**, *58*, 1526–1537. [\[CrossRef\]](#)
17. Trache, D.; Tarchoun, A.F.; Derradji, M.; Hamidon, T.S.; Masruchin, N.; Brosse, N.; Hussin, M.H. Nanocellulose: From Fundamentals to Advanced Applications. *Front. Chem.* **2020**, *8*, 392. [\[CrossRef\]](#) [\[PubMed\]](#)
18. Kang, Q.; Appels, L.; Tan, T.; Dewil, R. Bioethanol from Lignocellulosic Biomass: Current Findings Determine Research Priorities. *Sci. World J.* **2014**, *2014*, 298153. [\[CrossRef\]](#) [\[PubMed\]](#)
19. Bušić, A.; Marđetko, N.; Kundas, S.; Morzak, G.; Belskaya, H.; Šantek, M.I.; Komes, D.; Novak, S.; Šantek, B. Bioethanol Production from Renewable Raw Materials and Its Separation and Purification: A Review. *Food Technol. Biotechnol.* **2018**, *56*, 289–311. [\[CrossRef\]](#)
20. Hanaki, K.; Portugal-Pereira, J. The Effect of Biofuel Production on Greenhouse Gas Emission Reductions. In *Biofuels and Sustainability. Science for Sustainable Societies*; Takeuchi, K., Shiroyama, H., Saito, O., Matsuura, M., Eds.; Springer: Tokyo, Japan, 2018; pp. 53–71.
21. Clauser, N.M.; González, G.; Mendieta, C.M.; Kruiyanski, J.; Area, M.C.; Vallejos, M.E. Biomass Waste as Sustainable Raw Material for Energy and Fuels. *Sustainability* **2021**, *13*, 794. [\[CrossRef\]](#)
22. Guo, Y.; Zhang, Y.; Zheng, D.; Li, M.; Yue, J. Isolation and characterization of nanocellulose crystals via acid hydrolysis from agricultural waste-tea stalk. *Int. J. Biol. Macromol.* **2020**, *163*, 927–933. [\[CrossRef\]](#) [\[PubMed\]](#)

23. Inkrod, C.; Raita, M.; Laosiripojana, N.; Champreda, V. Characteristics of Lignin Extracted from Different Lignocellulosic Materials via Organosolv Fractionation. *Bioenergy Res.* **2018**, *11*, 277–290. [[CrossRef](#)]
24. Chin, D.W.K.; Lim, S.; Pang, Y.L.; Lim, C.H.; Shuit, S.H.; Lee, K.M.; Chong, C.T. Effects of Organic Solvents on the Organosolv Pretreatment of Degraded Empty Fruit Bunch for Fractionation and Lignin Removal. *Sustainability* **2021**, *13*, 6757. [[CrossRef](#)]
25. Pelaez-Samaniego, M.R.; Yadama, V.; Lowell, E.; Espinoza-Herrera, R. A review of wood thermal pretreatments to improve wood composite properties. *Wood Sci. Technol.* **2013**, *47*, 1285–1319. [[CrossRef](#)]
26. Klamrassamee, T.; Champreda, V.; Reunglek, V.; Laosiripojana, N. Comparison of homogeneous and heterogeneous acid promoters in single-step aqueous-organosolv fractionation of eucalyptus wood chips. *Bioresour. Technol.* **2013**, *147*, 276–284. [[CrossRef](#)] [[PubMed](#)]
27. Ferreira, F.V.; Mariano, M.; Rabelo, S.C.; Gouveia, R.F.; Lona, L.M.F. Isolation and surface modification of cellulose nanocrystals from sugarcane bagasse waste: From a micro- to a nano-scale view. *Appl. Surf. Sci.* **2018**, *436*, 1113–1122. [[CrossRef](#)]
28. Mân Vu, T.H.; Pakkanen, H.; Alén, R. Delignification of bamboo (*Bambusa procera* acher): Part 1. Kraft pulping and the subsequent oxygen delignification to pulp with a low kappa number. *Ind. Crops Prod.* **2004**, *19*, 49–57. [[CrossRef](#)]
29. Mussatto, S.I.; Rocha, G.J.M.; Roberto, I.C. Hydrogen peroxide bleaching of cellulose pulps obtained from brewer's spent grain. *Cellulose* **2008**, *15*, 641–649. [[CrossRef](#)]
30. Muangmeesri, S.; Li, N.; Georgouvelas, D.; Ouagne, P.; Placet, V.; Mathew, A.P.; Samec, J.S.M. Holistic Valorization of Hemp through Reductive Catalytic Fractionation. *ACS Sustain. Chem. Eng.* **2021**, *9*, 17207–17213. [[CrossRef](#)]
31. Dong, X.M.; Revol, J.-F.; Gray, D.G. Effect of microcrystallite preparation conditions on the formation of colloid crystals of cellulose. *Cellulose* **1998**, *5*, 19–32. [[CrossRef](#)]
32. Börjesson, M.; Westman, G. Crystalline Nanocellulose—Preparation, Modification, and Properties. In *Cellulose—Fundamental Aspects and Current Trends*; IntechOpen: London, UK, 2015.
33. Saïd Azizi Samir, M.A.; Alloin, F.; Paillet, M.; Dufresne, A. Tangling Effect in Fibrillated Cellulose Reinforced Nanocomposites. *Macromolecules* **2004**, *37*, 4313–4316. [[CrossRef](#)]
34. Kusmono; Listyanda, R.F.; Wildan, M.W.; Iman, M.N. Preparation and characterization of cellulose nanocrystal extracted from ramie fibers by sulfuric acid hydrolysis. *Heliyon* **2020**, *6*, e05486. [[CrossRef](#)] [[PubMed](#)]
35. Wulandari, W.T.; Rochliadi, A.; Arcana, I.M. Nanocellulose prepared by acid hydrolysis of isolated cellulose from sugarcane bagasse. *IOP Conf. Ser. Mater. Sci. Eng.* **2016**, *107*, 012045. [[CrossRef](#)]
36. Zianor Azrina, Z.A.; Beg, M.D.H.; Rosli, M.Y.; Ramli, R.; Junadi, N.; Alam, A.K.M.M. Spherical nanocrystalline cellulose (NCC) from oil palm empty fruit bunch pulp via ultrasound assisted hydrolysis. *Carbohydr. Polym.* **2017**, *162*, 115–120. [[CrossRef](#)] [[PubMed](#)]
37. Mehanny, S.; Magd, E.E.A.-E.; Ibrahim, M.; Farag, M.; Gil-San-Millan, R.; Navarro, J.; Habbak, A.E.H.E.; El-Kashif, E. Extraction and characterization of nanocellulose from three types of palm residues. *J. Mater. Res. Technol.* **2021**, *10*, 526–537. [[CrossRef](#)]
38. Holilah, H.; Bahruji, H.; Ediati, R.; Asranudin, A.; Jalil, A.A.; Piluharto, B.; Nugraha, R.E.; Prasetyoko, D. Uniform rod and spherical nanocrystalline celluloses from hydrolysis of industrial pepper waste (*Piper nigrum* L.) using organic acid and inorganic acid. *Int. J. Biol. Macromol.* **2022**, *204*, 593–605. [[CrossRef](#)]
39. Gong, J.; Li, J.; Xu, J.; Xiang, Z.; Mo, L. Research on cellulose nanocrystals produced from cellulose sources with various polymorphs. *RSC Adv.* **2017**, *7*, 33486–33493. [[CrossRef](#)]
40. Csiszar, E.; Kalic, P.; Kobol, A.; Ferreira Ede, P. The effect of low frequency ultrasound on the production and properties of nanocrystalline cellulose suspensions and films. *Ultrason. Sonochem.* **2016**, *31*, 473–480. [[CrossRef](#)]
41. El Achaby, M.; El Miri, N.; Aboulkas, A.; Zahouily, M.; Bilal, E.; Barakat, A.; Solhy, A. Processing and properties of eco-friendly bio-nanocomposite films filled with cellulose nanocrystals from sugarcane bagasse. *Int. J. Biol. Macromol.* **2017**, *96*, 340–352. [[CrossRef](#)]
42. Khawas, P.; Deka, S.C. Isolation and characterization of cellulose nanofibers from culinary banana peel using high-intensity ultrasonication combined with chemical treatment. *Carbohydr. Polym.* **2016**, *137*, 608–616. [[CrossRef](#)]
43. Kargarzadeh, H.; Ahmad, I.; Abdullah, I.; Dufresne, A.; Zainudin, S.Y.; Sheltami, R.M. Effects of hydrolysis conditions on the morphology, crystallinity, and thermal stability of cellulose nanocrystals extracted from kenaf bast fibers. *Cellulose* **2012**, *19*, 855–866. [[CrossRef](#)]
44. Listyanda, R.F.; Kusmono Wildan, M.W.; Iman, M.N. Extraction and characterization of nanocrystalline cellulose (NCC) from ramie fiber by sulphuric acid hydrolysis. *AIP Conf. Proc.* **2020**, *2217*, 030069.
45. Asrofi, M.; Abral, H.; Kasim, A.; Pratoto, A. XRD and FTIR Studies of Nanocrystalline Cellulose from Water Hyacinth (*Eichornia crassipes*) Fiber. *J. Metastable Nanocrystalline Mater.* **2017**, *29*, 9–16. [[CrossRef](#)]
46. Sun, J.X.; Xu, F.; Sun, X.F.; Xiao, B.; Sun, R.C. Physico-chemical and thermal characterization of cellulose from barley straw. *Polym. Degrad. Stab.* **2005**, *88*, 521–531. [[CrossRef](#)]
47. Sungsinchai, S. Production and Characterization of Nanocellulose and Its Applications as Food Thickener and Emulsifier. In *Chemical Engineering*; Kasersart Uiniversity: Bangkok, Thailand, 2021.
48. Burhani, D.; Septevani, A.A.; Setiawan, R.; Djannah, L.M.; Putra, M.A.; Kusumah, S.S.; Sondari, D. Self-Assembled Behavior of Ultralightweight Aerogel from a Mixture of CNC/CNF from Oil Palm Empty Fruit Bunches. *Polymers* **2021**, *13*, 2649. [[CrossRef](#)] [[PubMed](#)]

49. Casas, A.; Alonso, M.V.; Oliet, M.; Santos, T.M.; Rodriguez, F. Characterization of Cellulose regenerated from solutions of pine and eucalyptus woods in 1-allyl-3-methylimidazolium chloride. *Carbohydr. Polym.* **2013**, *92*, 1946–1952. [[CrossRef](#)] [[PubMed](#)]
50. Ingole, V.H.; Vuherer, T.; Maver, U.; Vinchurkar, A.; Ghule, A.V.; Kokol, V. Mechanical Properties and Cytotoxicity of Differently Structured Nanocellulose-hydroxyapatite Based Composites for Bone Regeneration Application. *Nanomaterials* **2019**, *10*, 25. [[CrossRef](#)]
51. Sungsinchai, S.; Niamnuay, C.; Seubsai, A.; Prapainainar, P.; Wattanapan, P.; Thakhiew, W.; Raghavan, V.; Devahastin, S. Comparative evaluation of the effect of microfluidisation on physicochemical properties and usability as food thickener and Pickering emulsifier of autoclaved and Tempo-oxidized nanofibrillated cellulose. *Int. J. Food Sci. Technol.* **2021**, *56*, 4298–4315. [[CrossRef](#)]
52. Murakami, T. Creating Better Social Acceptance for Electric Power Infrastructure. *ERIA Res. Proj. Rep.* **2017**, *2017*, 3–18.
53. Andres, R.J.; Boden, T.A.; Bréon, F.M.; Ciais, P.; Davis, S.; Erickson, D.; Gregg, J.S.; Jacobson, A.; Marland, G.; Miller, J.; et al. A synthesis of carbon dioxide emissions from fossil-fuel combustion. *Biogeosciences* **2012**, *9*, 1845–1871. [[CrossRef](#)]
54. Raghuvanshi, S.; Babu, B.V. Biofiltration for removal of methyl isobutyl ketone (MIBK): Experimental studies and kinetic modelling. *Environ. Technol.* **2010**, *31*, 29–40. [[CrossRef](#)]
55. Tsai, W.T. Fate of Chloromethanes in the Atmospheric Environment: Implications for Human Health, Ozone Formation and Depletion, and Global Warming Impacts. *Toxics* **2017**, *5*, 23. [[CrossRef](#)]
56. Heijungs, R.; Koning, A.D. *Improvement of LCA Characterization Factors and LCA Practice for Metals*; Institute of Environmental Sciences—Leiden University: Apeldoorn, The Netherlands, 2004.
57. Stringer, D.A. *Joint Assessment Commodity of Chemicals No. 8 Methyl Isobutyl Ketone CAS: 108-10-1*; ECETOC: Brussels, Belgium, 1987.
58. Chipman, K. *Environmental Health Criteria 117 Methyl Isobutyl Ketone*; World Health Organization: Geneva, Switzerland, 1990.
59. Atilgan, B.; Azapagic, A. Assessing the Environmental Sustainability of Electricity Generation in Turkey on a Life Cycle Basis. *Energies* **2016**, *9*, 31. [[CrossRef](#)]
60. Albanese, S.; Cicchella, D. Legacy Problems in Urban Geochemistry. *Elements* **2012**, *8*, 423–428. [[CrossRef](#)]
61. Hameed, S.; Dignon, J. Global Emissions of Nitrogen and Sulfur Oxides in Fossil Fuel Combustion 1970–1986. *J. Air Waste Manag. Assoc.* **2012**, *42*, 159–163. [[CrossRef](#)]
62. Amoatey, P.; Omidvarborna, H.; Baawain, M.S.; Al-Mamun, A. Emissions and exposure assessments of SOX, NOX, PM10/2.5 and trace metals from oil industries: A review study (2000–2018). *Process. Saf. Environ. Prot.* **2019**, *123*, 215–228. [[CrossRef](#)]
63. Johnson, W., Jr. Safety assessment of MIBK (methyl isobutyl ketone). *Int. J. Toxicol.* **2004**, *23*, 29–57. [[PubMed](#)]
64. Sluiter, J.B.; Ruiz, R.O.; Scarlata, C.J.; Sluiter, A.D.; Templeton, D.W. Compositional analysis of lignocellulosic feedstocks. 1. Review and description of methods. *J. Agric. Food. Chem.* **2010**, *58*, 9043–9053. [[CrossRef](#)]
65. Michel, K.; Sluiter, J.; Payne, C.; Ness, R.; Thornton, B.; Reed, M.; Schwartz, A.; Wolfrum, E. *Determination of Cellulosic Glucan Content in Starch Containing Feedstocks*; National Renewable Energy Laboratory: Golden, CO, USA, 2021.
66. Peng, Y.; Gardner, D.J.; Han, Y.; Cai, Z.; Tshabalala, M.A. Influence of drying method on the surface energy of cellulose nanofibrils determined by inverse gas chromatography. *J. Colloid Interface Sci.* **2013**, *405*, 85–95. [[CrossRef](#)]
67. Kaushik, M.; Chen, W.C.; Ven, T.G.M.V.D.; Moores, A. An Improved Methodology for Imaging Cellulose Nanocrystals by Transmission Electron Microscopy. *Nord. Pulp Pap. Res. J.* **2014**, *25*, 77–84. [[CrossRef](#)]
68. Segal, L.; Creely, J.J.; Martin, A.E.; Conrad, C.M. An Empirical Method for Estimating the Degree of Crystallinity of Native Cellulose using the X-ray Diffractometer. *Text. Res. J.* **1957**, *25*, 786–794.